Hybrid FE/BI Modeling of 3-D Doubly Periodic Structures Utilizing Triangular Prismatic Elements and an MPIE Formulation Accelerated by the Ewald Transformation

Thomas F. Eibert, *Member, IEEE*, John L. Volakis, *Fellow, IEEE*, Donald R. Wilton, *Fellow, IEEE*, and David R. Jackson, *Fellow, IEEE*

***Abstract*— In this paper, we present the formulation of a finite-element/boundary-integral method for the analysis of three-dimensional doubly periodic structures based on arbitrary nonorthogonal lattice configurations. The method starts from a functional description of the field problem where only a single unit cell of the array is considered. This unit cell is meshed with triangular prismatic volume elements and the electric field intensity is discretized with edge-based expansion functions. On the sidewalls of the unit cell, phase boundary conditions are employed to relate the fields on opposing walls of the unit cell. On the top and/or bottom unit-cell planar surfaces, the mesh is terminated using a mixed potential integral equation. The required space-domain periodic Green's function is calculated after applying the Ewald transformation to convert the slowly converging series representation into two rapidly converging series. The method is validated for simple slot and strip frequency-selective surfaces as well as microstrip dipole arrays. More complex geometries investigated are slot-coupled microstrip patches, photonic bandgap materials, and the so-called "artificial puck plate" frequency-selective surface bandpass structure.**

***Index Terms*—Arrays, finite elements, frequency-selective surfaces, hybrid methods, integral equations, periodic structures.**

I. Introduction

BY applying appropriate periodicity conditions, the computational domain of infinite periodic structures can be reduced to a single unit cell. Previous analyses have mainly been restricted to the application of Floquet's theorem to construct periodic Green's functions in the context of integral equation formulations. An overview of techniques for the analysis of single-layer frequency-selective surfaces (FSS's) based on spectral-domain integral equation formulations is given in [1], together with a discussion of cascading approaches for multilayered structures. Further examples of spectral-domain formulations involving the analysis of multilayered planar structures such as aperture-coupled microstrip patches are described in [2], [3]. A difficulty with spectral-domain formulations of periodic Green's functions is the slow convergence of the Floquet-mode series. Therefore, acceleration techniques like the method of Singh as applied in [4] or the Shanks transformation [5] must be used in conjunction with mixed-potential integral equation (MPIE) formulations. An overview of acceleration techniques is given in [6]. Improved convergence behavior can be obtained by applying the so-called Ewald transformation, which was suggested by P. P. Ewald in his thesis [7] and later extended to deal with skewed three-dimensional crystal lattices [8]. A numerical implementation of the Ewald transformation for two-dimensional lattices was described in [9]. In [10], the Ewald transformation was used to accelerate convergence for doubly periodic arrays of rectangular apertures in metallic screens. In [11], a volume integral equation formulation for the analysis of three-dimensional periodic structures embedded in multilayered media is described. The computational complexity of this approach can be considerable unless advantage is taken of the Toeplitz properties of the coupling matrices resulting from regular discretizations.

Fully three-dimensional modeling capabilities can be achieved by using hybrid finite element (FE)/boundary integral (BI) methods. However, the formulation is also useful for the calculation of two-dimensional problems, as shown in [12], where a two-dimensional FE/BI approach was suggested for the analysis of plane-wave diffraction by gratings of arbitrary cross section. Three-dimensional approaches for the analysis of doubly periodic structures are presented in [13]–[15]. Both of these methods are based on FE modeling employing tetrahedral meshes and spectral-domain Floquet-mode expansions of the BI fields. In this paper, we propose a hybrid FE/BI method employing distorted triangular prismatic elements for volume tessellation and an MPIE formulation in the spatial domain for mesh truncation. The triangular prismatic elements provide full geometrical adaptability in the plane of the triangles and structured meshing along the depth of the cell. Because structured gridding is used for volume meshing, simple automatic mesh generation can be employed

Manuscript received April 2, 1998. This work was supported in part by the Office of Naval Research (ONR-313) through the Naval Air Warfare Center Aircraft Division (NAWCAD 4.5.5.5) Contract with Sanders, A Lockheed Martin Corporation. The work of T. P. Eibert was supported by the "German Academic Exchange Service (DAAD)."

T. F. Eibert and J. L. Volakis are with the Radiation Laboratory, Electrical Engineering and Computer Science Department, University of Michigan, Ann Arbor MI 48109-2122 USA.

D. R. Wilton and D. R. Jackson are with the Department of Electrical and Computer Engineering, University of Houston, Houston, TX 77204 USA.

Publisher Item Identifier S 0018-926X(99)04830-9.

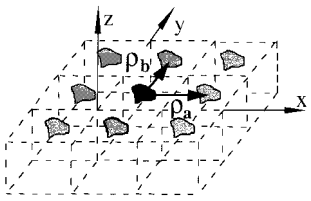

Fig. 1. Infinite periodic structure.

for the analysis of multilayered FSS structures. Prismatic elements facilitate the performance of design studies since geometry meshing may be accomplished by varying a few external parameters without the need to manually regrid the geometry at each design iteration. Another important aspect of the present approach is the use of the Ewald acceleration technique for evaluating the periodic Green's function.

In Section II, the formulation of the method is given starting from a functional description of the field problem. The majority of this section is devoted to the FE implementation involving the phase boundary conditions as well as the BI formulation with the Ewald transformation. Results for a variety of periodic structures, including antenna arrays and artificial dielectrics, are presented in Section III.

II. Formulation

A. Weak Formulation of the Field Problem

We consider the periodic structure illustrated in Fig. 1 for time harmonic electromagnetic fields (an $e^{j\omega t}$ time dependence is assumed and suppressed throughout). The array is assumed to be periodic in the xy-plane and the (m,n) cell of the array is obtained by shifting the $(0,0)$ cell through the relation

$$\boldsymbol{\rho}_{mn} = m\boldsymbol{\rho}_a + n\boldsymbol{\rho}_b. \tag{1}$$

Here, $\boldsymbol{\rho}_a$, $\boldsymbol{\rho}_b$ are the lattice vectors parallel to the xy-plane. For periodic excitation of the array with a linear phase factor, the fields in the array obey the periodicity conditions

$$\begin{aligned}\boldsymbol{E}(\boldsymbol{r}+m\boldsymbol{\rho}_a+n\boldsymbol{\rho}_b) &= \boldsymbol{E}(\boldsymbol{r})e^{-j\boldsymbol{k}_{t00}\cdot(m\boldsymbol{\rho}_a+n\boldsymbol{\rho}_b)}\\ \boldsymbol{H}(\boldsymbol{r}+m\boldsymbol{\rho}_a+n\boldsymbol{\rho}_b) &= \boldsymbol{H}(\boldsymbol{r})e^{-j\boldsymbol{k}_{t00}\cdot(m\boldsymbol{\rho}_a+n\boldsymbol{\rho}_b)}\end{aligned} \tag{2}$$

with

$$\begin{aligned}\boldsymbol{k}_{t00} &= k_{x00}\hat{\boldsymbol{x}} + k_{y00}\hat{\boldsymbol{y}}\\ &= \pm(k_0\sin\vartheta_0\cos\varphi_0\hat{\boldsymbol{x}} + k_0\sin\vartheta_0\sin\varphi_0\hat{\boldsymbol{y}}).\end{aligned} \tag{3}$$

In (3), k_0 is the wavenumber of free space and ϑ_0, φ_0 are the spherical coordinates corresponding to the scan angles of a phased array (positive sign) or the arrival angles of an incident plane wave (negative sign). The pertinent finite-element functional is

$$\begin{aligned}F(\boldsymbol{E}_{\rm ad},\boldsymbol{E}) = \iiint_V \Big[&\frac{1}{\mu_r}(\nabla\times\boldsymbol{E}_{\rm ad})\cdot(\nabla\times\boldsymbol{E})\\ &- k_0^2\varepsilon_r\boldsymbol{E}_{\rm ad}\cdot\boldsymbol{E} + jk_0Z_0\boldsymbol{E}_{\rm ad}\cdot\boldsymbol{J}^{\rm int}\Big]\,dv\\ &+ jk_0Z_0\iint_S \boldsymbol{E}_{\rm ad}\cdot(\boldsymbol{H}\times\hat{\boldsymbol{n}})\,ds\end{aligned} \tag{4}$$

where $\boldsymbol{E}_{\rm ad}$ is the solution of the adjoint field problem, $\boldsymbol{J}^{\rm int}$ denotes an excitation current interior to the FE domain, S represents the bounding surface of the FE domain, $\hat{\boldsymbol{n}}$ is the unit surface normal directed out of the FE domain, and Z_0 is the wave impedance of free space. It is well known that $\boldsymbol{H}\times\hat{\boldsymbol{n}}$ in the surface integral of (4) must be replaced by an expression in terms of $\boldsymbol{E}$. This is the process of mesh truncation and, as noted earlier, the BI will be employed for this purpose. Restricting ourselves to planar mesh truncation surfaces, the appropriate BI relation in MPIE form is given by

$$\begin{aligned}\boldsymbol{H} = -2j\frac{k_0}{Z_0}\Bigg[&\iint_S G(\boldsymbol{r},\boldsymbol{r}_s)(\boldsymbol{E}\times\hat{\boldsymbol{n}})\,ds\\ &+ \frac{1}{k_0^2}\nabla\iint_S G(\boldsymbol{r},\boldsymbol{r}_s)\nabla_s\cdot(\boldsymbol{E}\times\hat{\boldsymbol{n}})\,ds\Bigg] + \boldsymbol{H}^{\rm exc}\end{aligned} \tag{5}$$

where

$$G(\boldsymbol{r},\boldsymbol{r}_s) = \exp(-jk_0|\boldsymbol{r}-\boldsymbol{r}_s|)/(4\pi|\boldsymbol{r}-\boldsymbol{r}_s|)$$

is the scalar free-space Green's function and $\boldsymbol{H}^{\rm exc}$ is an excitation field (calculated in the presence of a metallic interface for a periodic aperture S). Also, $\nabla_s\cdot$ denotes the surface divergence operator. Substituting (5) into (4) and invoking the divergence theorem results in

$$\begin{aligned}&F(\boldsymbol{E}_{\rm ad},\boldsymbol{E})\\ &= \iiint_V \Big[\frac{1}{\mu_r}(\nabla\times\boldsymbol{E}_{\rm ad})\cdot(\nabla\times\boldsymbol{E})\\ &\quad - k_0^2\varepsilon_r\boldsymbol{E}_{\rm ad}\cdot\boldsymbol{E} + jk_0Z_0\boldsymbol{E}_{\rm ad}\cdot\boldsymbol{J}^{\rm int}\Big]\,dv\\ &\quad - 2k_0^2\iint_S\iint_S G(\boldsymbol{r},\boldsymbol{r}_s)\Big[(\hat{\boldsymbol{n}}\times\boldsymbol{E}_{\rm ad}(\boldsymbol{r}))\cdot(\hat{\boldsymbol{n}}\times\boldsymbol{E}(\boldsymbol{r}_s))\\ &\quad - \frac{1}{k_0^2}\nabla_s\cdot(\hat{\boldsymbol{n}}\times\boldsymbol{E}_{\rm ad}(\boldsymbol{r}))\nabla_s\cdot(\hat{\boldsymbol{n}}\times\boldsymbol{E}(\boldsymbol{r}_s))\Big]\,ds_s\,ds\\ &\quad + jk_0Z_0\iint_S(\hat{\boldsymbol{n}}\times\boldsymbol{E}_{\rm ad}(\boldsymbol{r}))\cdot\boldsymbol{H}^{\rm exc}(\boldsymbol{r})\,ds\end{aligned} \tag{6}$$

which is the exact functional description of the periodic field problem. Based on the periodicity condition (2), the solution domain can be restricted to a single unit cell of the periodic array. However, by this procedure additional (vertical) boundaries of the solution domain are created. The phase boundary conditions (PBC's), (2), must be employed on these to obtain a unique solution of the field problem. Moreover, the free-space Green's function $G(\boldsymbol{r},\boldsymbol{r}_s)$ must be replaced by the appropriate Green's function $G_p(\boldsymbol{r},\boldsymbol{r}_s)$ for a periodic array of δ-sources in free space.

B. Finite Elements

For the discretization of the volume integrals in (6) we employ edge-based basis functions on triangular prismatic elements as described in [16] and [17]. The resulting meshes give full modeling flexibility in the transverse direction but

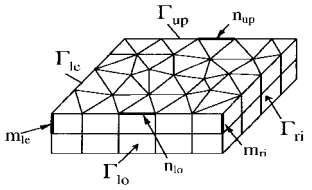

Fig. 2. FE mesh consisting of triangular prisms.

are structured in the direction normal to the triangular cross sections. As a result, mesh generation with triangular prisms is much simpler in comparison to tetrahedral meshes and is well-suited for designing layered periodic structures. As an example, a simplified FE mesh with triangular prisms for a unit cell of an infinite periodic array is illustrated in Fig. 2. The four vertical walls of the FE mesh are designated as $\Gamma_{\rm le}$, $\Gamma_{\rm ri}$, $\Gamma_{\rm lo}$, $\Gamma_{\rm up}$, where $\Gamma_{\rm le}$ and $\Gamma_{\rm lo}$ are assumed to be the sidewalls opposite to $\Gamma_{\rm ri}$ and $\Gamma_{\rm up}$, respectively. A possible imposition of the PBC's on the vertical walls of the FE mesh was discussed in detail in [14] and [15]. The basic observation in this context is that the fields on a vertical boundary of the FE mesh are related to the fields on the opposite boundary by (2) through a phase relation. If e_m is the unknown field at an edge on one of the vertical walls, the value e_n of the field at the corresponding edge on the opposite sidewall is given by

$$e_n = e_m e^{-j\boldsymbol{k}_{t00}\cdot\Delta\boldsymbol{r}} \tag{7}$$

where $\Delta\boldsymbol{r}(=\boldsymbol{\rho}_a$ or $\boldsymbol{\rho}_b)$ is the vector joining the two edges. This relation requires that the surface meshes of the opposite vertical walls be identical, and this is easily satisfied using prismatic meshes, but not so easily done using tetrahedral meshes. In our implementation, we eliminate the unknowns on the surfaces $\Gamma_{\rm ri}$ and $\Gamma_{\rm up}$ by relating them to those on $\Gamma_{\rm le}$ and $\Gamma_{\rm lo}$ using (7). For example, in Fig. 2 the unknown field at edge $n_{\rm up}$ is replaced by the unknown field at edge $n_{\rm lo}$. Similarly, the unknown field at edge $m_{\rm ri}$ is replaced by the unknown field at edge $m_{\rm le}$. For the construction of the FE system matrix, this means that the corresponding matrix elements are modified and condensed according to (7) as described in [14] and [15]. However, in our implementation, matrix condensation is performed during the generation of the matrix and not as a second step. This allows for the most efficient sparse matrix storage.

C. Boundary Integral

The edge-based basis functions for triangular prisms reduce to Rao–Wilton–Glisson basis functions [18] on the top and bottom triangular surface meshes of the periodic unit cell. Therefore, these basis functions are used to represent the field in the boundary integral in (6). In the spatial domain, the periodic Green's function $G_p(\boldsymbol{r},\boldsymbol{r}_s)$ has the form

$$G_p(\boldsymbol{r},\boldsymbol{r}_s) = \sum_{m=-\infty}^{\infty}\sum_{n=-\infty}^{\infty} e^{-j\boldsymbol{k}_{t00}\cdot\boldsymbol{\rho}_{mn}}\frac{e^{-jk_0R_{mn}}}{4\pi R_{mn}} \tag{8}$$

where

$$R_{mn} = |\boldsymbol{r}-\boldsymbol{r}_s-\boldsymbol{\rho}_{mn}|. \tag{9}$$

In the spectral domain, $G_p(\boldsymbol{r},\boldsymbol{r}_s)$ becomes

$$G_p(\boldsymbol{r},\boldsymbol{r}_s) = \sum_{m=-\infty}^{\infty}\sum_{n=-\infty}^{\infty}\frac{e^{-j\boldsymbol{k}_{tmn}\cdot(\boldsymbol{\rho}-\boldsymbol{\rho}_s)}}{2jAk_{zmn}}e^{-jk_{zmn}|z-z_s|} \tag{10}$$

where $A = |\boldsymbol{\rho}_a\times\boldsymbol{\rho}_b|$ is the cross-sectional area of the unit cell

$$\boldsymbol{r} = \boldsymbol{\rho} + z\hat{\boldsymbol{z}} \tag{11}$$

$$\boldsymbol{k}_{tmn} = \boldsymbol{k}_{t00} + \frac{2\pi}{A}[m(\boldsymbol{\rho}_b\times\hat{\boldsymbol{z}}) + n(\hat{\boldsymbol{z}}\times\boldsymbol{\rho}_a)] \tag{12}$$

is the so-called reciprocal lattice vector, and

$$k_{zmn} = \sqrt{k_0^2 - \boldsymbol{k}_{tmn}\cdot\boldsymbol{k}_{tmn}} \tag{13}$$

where $\mathrm{Re}\,(k_{zmn}) \geq 0$, $\mathrm{Im}\,(k_{zmn}) \leq 0$. In many cases, the spectral-domain representation (10) has satisfactory convergence behavior if applied in a spectral-domain formulation of the integral equation. However, for arbitrary array configurations analyzed in the space domain, having strongly as well as weakly coupled array elements, it is necessary to have a representation that converges faster than either (8) or (10). This can be achieved by employing the so-called Ewald transformation originally proposed by Ewald for modeling optical and electrostatic potentials in three-dimensional ion lattices [7], [8]. An application of the Ewald transformation for time-harmonic fields of two-dimensional lattices was presented in [9]. The formulation there is restricted to rectangular lattices, but the transformation is also applicable to skewed lattices by employing the reciprocal lattice representation used here. The Ewald transformation starts from the spatial domain representation of the periodic Green's function (8) and makes use of the identity

$$\frac{e^{-jk_0R_{mn}}}{R_{mn}} = \frac{2}{\sqrt{\pi}}\int_0^{\infty} e^{-R_{mn}^2s^2+\frac{k_0^2}{4s^2}}\,ds \tag{14}$$

where s is a complex variable. In order that the integrand converges as $s\to 0$ for a wavenumber k_0 with an arbitrary amount of loss, the path is chosen so that $\arg(s) = \frac{\pi}{4}$ as $s\to 0$. In order to have convergence as $s\to\infty$, the path is chosen so that $-\pi/4 \leq \arg(s) \leq \pi/4$. Next, (14) is substituted into (8) and the parameter E is introduced to split the integral into two terms, as

$$G_p(\boldsymbol{r},\boldsymbol{r}_s) = G_{p1}(\boldsymbol{r},\boldsymbol{r}_s) + G_{p2}(\boldsymbol{r},\boldsymbol{r}_s) \tag{15}$$

where

$$G_{p1}(\boldsymbol{r},\boldsymbol{r}_s) = \frac{1}{4\pi}\sum_{m=-\infty}^{\infty}\sum_{n=-\infty}^{\infty} e^{-j\boldsymbol{k}_{t00}\cdot\boldsymbol{\rho}_{mn}} \times\frac{2}{\sqrt{\pi}}\int_0^{E} e^{-R_{mn}^2s^2+\frac{k_0^2}{4s^2}}\,ds \tag{16}$$

$$G_{p2}(\boldsymbol{r},\boldsymbol{r}_s) = \frac{1}{4\pi}\sum_{m=-\infty}^{\infty}\sum_{n=-\infty}^{\infty} e^{-j\boldsymbol{k}_{t00}\cdot\boldsymbol{\rho}_{mn}} \times\frac{2}{\sqrt{\pi}}\int_E^{\infty} e^{-R_{mn}^2s^2+\frac{k_0^2}{4s^2}}\,ds. \tag{17}$$

Using the identity [19, eq. (7.4.34)]

$$\frac{2}{\sqrt{\pi}}\int_E^\infty e^{-R_{mn}^2 s^2+\frac{k_0^2}{4s^2}}\,ds = \frac{1}{2R_{mn}}\left[e^{-jk_0R_{mn}}\mathrm{erfc}\left(R_{mn}E-\frac{jk}{2E}\right) + e^{jk_0R_{mn}}\mathrm{erfc}\left(R_{mn}E+\frac{jk}{2E}\right)\right] \quad (18)$$

where erfc is the complementary error function, $G_{p2}(\boldsymbol{r},\boldsymbol{r}_s)$ can be written as

$$G_{p2}(\boldsymbol{r},\boldsymbol{r}_s)=\sum_{m=-\infty}^{\infty}\sum_{n=-\infty}^{\infty}\frac{e^{-j\boldsymbol{k}_{t00}\cdot\boldsymbol{\rho}_{mn}}}{8\pi R_{mn}} \times\left[e^{-jk_0R_{mn}}\mathrm{erfc}\left(R_{mn}E-\frac{jk}{2E}\right) + e^{jk_0R_{mn}}\mathrm{erfc}\left(R_{mn}E+\frac{jk}{2E}\right)\right] \quad (19)$$

which is essentially a "modified" spatial-domain portion of the periodic Green's function. Making use of the Poisson transformation, or alternatively following the procedure in [8], [9] employing a transformation formula for the series expansion of the ϑ-function, (16) is finally transformed to

$$G_{p1}(\boldsymbol{r},\boldsymbol{r}_s)=\sum_{m=-\infty}^{\infty}\sum_{n=-\infty}^{\infty}\frac{e^{-j\boldsymbol{k}_{tmn}\cdot(\boldsymbol{\rho}-\boldsymbol{\rho}_s)}}{4jAk_{zmn}} \times\left[e^{-jk_{zmn}|z-z_s|}\mathrm{erfc}\left(\frac{jk_{zmn}}{2E}-|z-z_s|E\right) + e^{jk_{zmn}|z-z_s|}\mathrm{erfc}\left(\frac{jk_{zmn}}{2E}+|z-z_s|E\right)\right] \quad (20)$$

where A is defined immediately after (10). Equation (20) can be identified as a "modified" spectral domain portion of the periodic Green's function. For planar BI surfaces, we can select $z=z_s=0$, giving the simplified form

$$G_{p1}(\boldsymbol{r},\boldsymbol{r}_s)=\sum_{m=-\infty}^{\infty}\sum_{n=-\infty}^{\infty}\frac{e^{-j\boldsymbol{k}_{tmn}\cdot(\boldsymbol{\rho}-\boldsymbol{\rho}_s)}}{2jAk_{zmn}}\,\mathrm{erfc}\left(\frac{jk_{zmn}}{2E}\right). \quad (21)$$

The two expressions (19) and (20) (or (21)) both converge exponentially (Gaussian convergence) and their computation is therefore very efficient, requiring only a few terms of the series. The parameter E controls the convergence rate. As E becomes larger, the spatial series (19) converges faster, while the spectral series (20) or (21) converges slower. The optimum parameter is that which makes the two series converge at the same rate, so that equal numbers of terms are required in the calculation of both series (assuming the same calculation time for corresponding terms in each of the two series). By analysis of the asymptotic behavior of the series terms, the optimum parameter E_{opt} is found to be [9]

$$E_{\mathrm{opt}}=\sqrt{\frac{\pi}{A}}. \quad (22)$$

Choosing this value for E and adjusting the summation limits so that the most dominant terms are kept, in almost all practical cases it is sufficient to include only nine summation terms in (19) and (20) [or (21)] (i.e., the summation limits are from -1 to $+1$), in which case the error level is usually less than 0.1%.

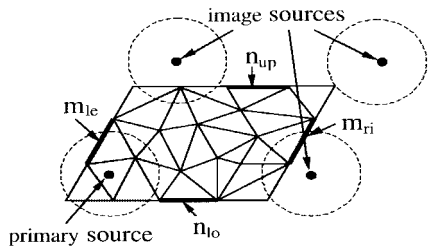

Fig. 3. Periodic image sources in triangular BI mesh.

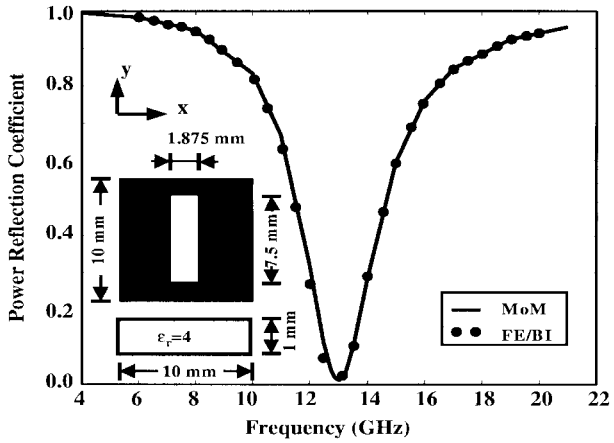

Fig. 4. TM power reflection from a one-layer slot array for a plane wave. $\vartheta_0=0°$, $\varphi_0=0°$.

For the implementation of the BI portion of the method, we apply the same phase transformations to the matrix elements associated with edges on Γ_{ri} and Γ_{up} (see Fig. 2) as done in the FE portion of the implementation (see Section II-B). We note that this approach is in contrast to the "overlapping elements" concept described in [12], [14], and [15]. However, our approach is advantageous in our spatial-domain MPIE formulation for treating the singularities of the Green's function. For our approach, source and test triangles are always inside the unit cell, therefore guaranteeing that the singularities of the neighboring array cells are never inside the test triangle. However, it is still necessary to carefully deal with the singularities of the neighboring array elements that are close to the test triangles, as illustrated in Fig. 3. The singularities, especially those of the self-cell elements, can be integrated using the formulas given in [20] and [21].

III. Results

For the validation of the method, we first analyzed the two simple FSS structures illustrated in Figs. 4 and 5. These were originally considered in [1]. The example in Fig. 4 is a slot FSS on a dielectric slab where the BI on the top surface is restricted to the slot aperture. In the diagram, we give the computed power reflection coefficient of the infinite slot array for an incident TM plane wave. A method of moments (MoM) formulation employing a multilayered Green's function was

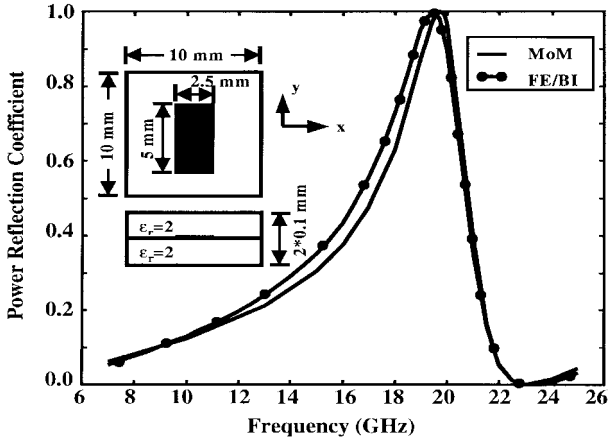

Fig. 5. TE power reflection from a one-layer strip array for a plane wave. $\vartheta_0 = 0°$, $\varphi_0 = 0°$.

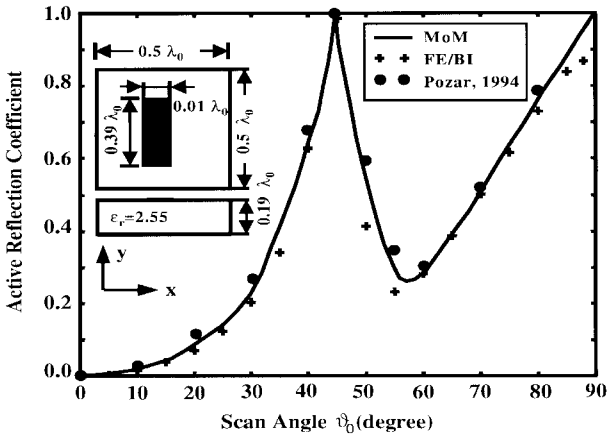

Fig. 6. TE active reflection coefficient for a microstrip dipole array as presented in [22]. $\varphi_0 = 0°$.

also developed during this study and is used to compare results for this and several other cases presented here. The FE/BI results were obtained using four subdivisions along the width of the slot and 15 subdivisions along the length of the slot. As seen, the results in Fig. 4 agree almost exactly with the MoM data. Compared to the results presented in [1], both curves are slightly shifted to higher frequencies.

The structure illustrated in Fig. 5 is a strip dipole FSS embedded in a dielectric layer. Again, our FE/BI results for the power reflection coefficient are compared to the corresponding results based on the MoM code for planar structures. In this case, the incident plane wave was TE polarized, parallel to the orientation of the strip dipoles. In contrast to the case of the slot array, the two resonance curves for the strip dipole array show a slight frequency shift of about 1%. We note that the FE/BI results were obtained using 16 subdivisons along the length and eight subdivisions along the width of the strip dipole. Further increases in the mesh density showed that the results were converged.

In Fig. 6, the active reflection coeffecient for a microstrip dipole array is depicted to demonstrate the antenna and scan modeling capabilities of our FE/BI method. The results compare very well to our own MoM results and those of [22].

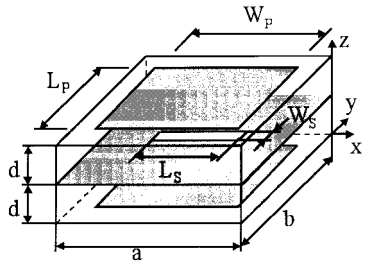

Fig. 7. FSS unit cell of aperture coupled microstrip patches as suggested in [2]. $\varepsilon_r = 2.2$, $d = 1.6$ mm, $a = 36.07$ mm, $b = 34.04$ mm.

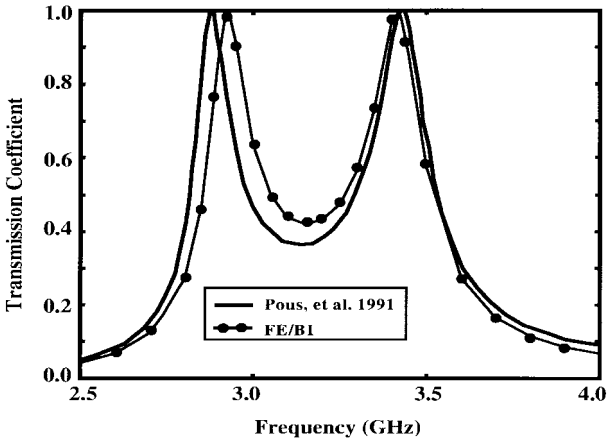

Fig. 8. TE transmission coefficient for the FSS structure in Fig. 7 compared to reference values from [2]. $L_s = 12$ mm, $W_s = 2$ mm, $W_p = 18$ mm, $L_p = 28$ mm, $\varphi_0 = 0°$, ϑ_0 varying from 57° to 32° for f varying from 2.5 to 4.0 GHz, according to waveguide measurement setup in [2].

A more complex FSS structure consisting of two slot-coupled microstrip patches [2] is given in Fig. 7. The modeling of this structure using MoM-based integral equation analysis is challenging, involving both coupled electric and magnetic surface current densities in layered media. However, modeling of the cell in Fig. 7 is a routine task in the FE/BI implementation. First, the geometric dimensions of the structure in Fig. 7 were designed to get a transmission coefficient curve with two separated resonance peaks as shown in Fig. 8. In [2], MoM results were compared to measurements; however, the measured resonance curves were obtained for a slot length of 12 mm whereas in the simulation a slot length of 11.2 mm was used to match the results. In our FE/BI simulations we found a good match to the resonance curves using the actual slot dimension of 12 mm. For the results shown in Fig. 9, the geometric dimensions were selected to obtain bandpass behavior of the transmission coefficient curve. Again, our FE/BI results are compared to MoM calculations as well as to measurements published in [2] and the discrepancies between the different curves are very small. It should be noted that the results in Figs. 8 and 9 were both obtained for incidence angles ϑ_0 which vary with frequency according to the waveguide measurements performed in [2].

As another example we consider the dielectric slab in Fig. 10 with embedded periodic material blocks. These lattices are often referred to as photonic bandgap materials. The diagram in Fig. 10 shows the reflection coefficient of

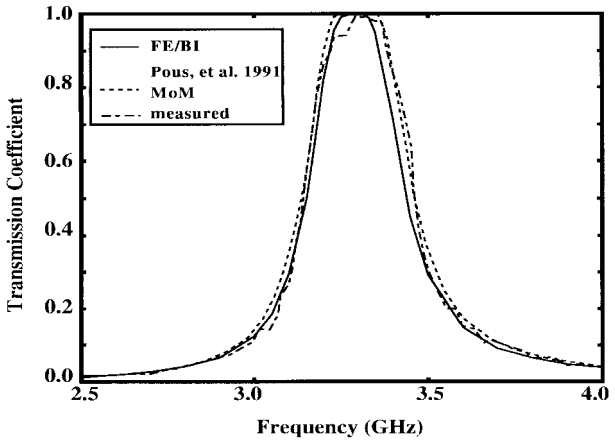

Fig. 9. TE transmission coefficient for the FSS structure in Fig. 7 compared to reference values from [2]. $L_s = 8$ mm, $W_s = 2$ mm, $W_p = 28$ mm, $L_p = 28$ mm, $\varphi_0 = 0°$, ϑ_0 varying from 57° to 32° for f varying from 2.5 to 4.0 GHz, according to waveguide measurement setup in [2].

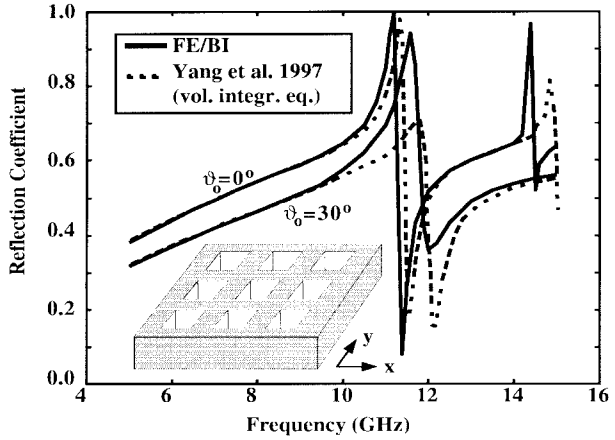

Fig. 10. TM plane wave reflection from a dielectric slab ($\varepsilon_r = 4$) with planarly embedded periodic material blocks ($\varepsilon_r = 10$) compared to reference values from [11]. Slab height: 0.2 cm, period: 2 × 2 cm, block side length: 1 × 1 cm, $\varphi_0 = 0°$.

plane waves incident on the slab with different incidence angles. The reflection coefficient curves exhibit the typical resonances of photonic bandgap materials. Compared to calculations obtained by a volume integral equation method [11], the first resonance is slightly shifted to a lower frequency whereas the frequency shift for the second resonance is larger. For TM waves with oblique incidence, the resonances shift to higher frequencies, in agreement with [11].

As a final example, Fig. 11 shows the unit cell for a so-called "artificial puck plate" FSS screen which was presented in [23] and analyzed in [13]. The basic FSS element is a dielectric-filled cylindrical waveguide with metallic walls and circular metallic irises in its apertures. On the top and bottom of the metallic plate, dielectric layers are placed for the optimization of the frequency behavior of the bandpass structure. The surface mesh used to grow the prismatic volume mesh of the unit cell is shown in Fig. 12. Our calculations are given in Fig. 13 and are compared to MoM data and FE/BI results based on a tetrahedral mesh published in [13]. As can

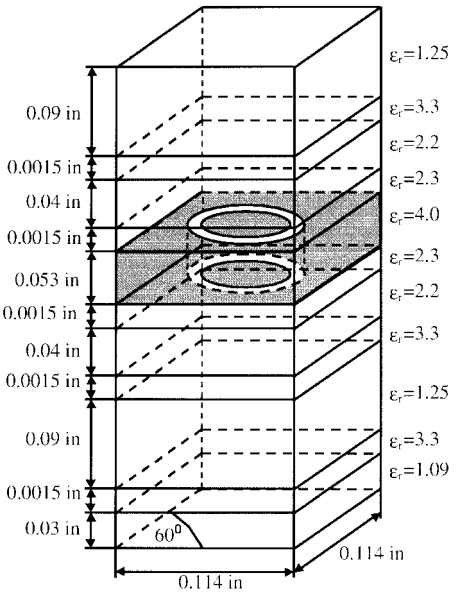

Fig. 11. Unit cell of "artificial puck plate" FSS as presented in [13].

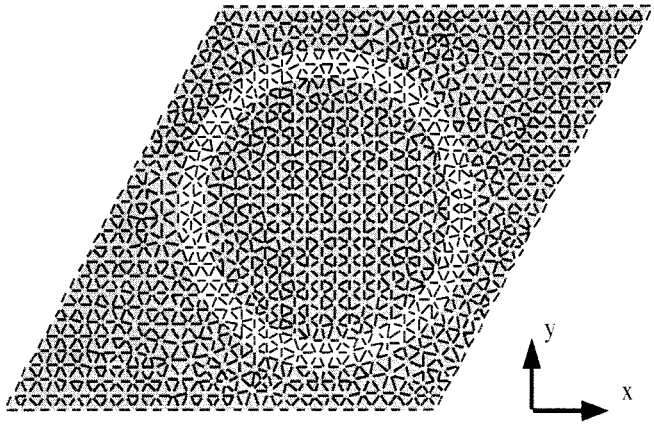

Fig. 12. Triangular surface mesh for the structure in Fig. 11.

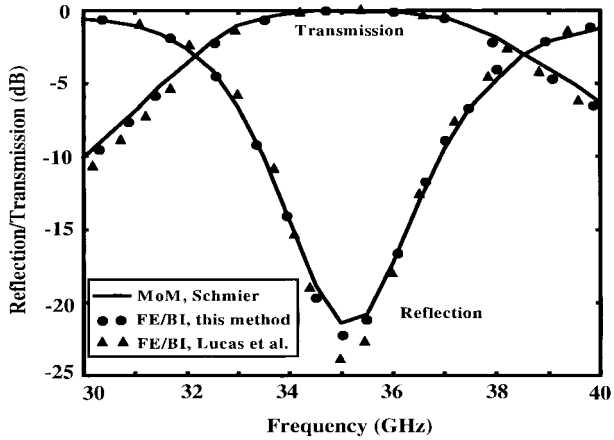

Fig. 13. TE reflection and transmission coefficients for bandpass structure in Fig. 11 compared to reference values from [13]. $\vartheta_0 = 0°$, $\varphi_0 = 0°$.

be seen, our FE/BI curves are closer to the MoM curves than the FE/BI results from [13]. This is likely due to our higher mesh density.

IV. Conclusion

In this paper, we presented a hybrid FE/BI method for the analysis of three-dimensional doubly periodic structures. The method can handle nonorthogonal (skew) lattices as well as arbitrary scan directions. The FE portion of the approach utilizes triangular prismatic volume meshes with edge-based basis functions for the electric field intensity. This meshing strategy provides for geometrical flexibility and ease of mesh generation for layered structures. On the top and/or bottom boundary planes of the unit cell, the mesh was truncated by a boundary integral, and a periodic phase boundary condition was employed on the sidewalls of the unit cell mesh. The BI was implemented using an MPIE formulation with the periodic Green's function in the space domain being computed via the Ewald acceleration technique, resulting in a rapidly converging series representation. The method was validated for simple slot and strip FSS as well as for microstrip dipole antenna arrays. Further results were shown for slot-coupled microstrip patches, photonic bandgap arrays, and a bandpass FSS based on a circular hollow waveguide with dielectric cover layers.

References

[1] R. Mittra, C. H. Chan, and T. Cwik, "Techniques for analyzing frequency selective surfaces—A review," in *Proc. IEEE*, vol. 76, no. 12, pp. 1593–1615, Dec. 1988.

[2] R. Pous and D. M. Pozar, "A frequency-selective surface using aperture-coupled microstrip patches," *IEEE Trans. Antennas Propagat.*, vol. 39, pp. 1763–1769, Dec. 1991.

[3] H. Aroudaki, V. Hansen, H.-P. Gemünd, and E. Kreysa, "Analysis of low-pass filters consisting of multiple stacked FSS's of different periodicities with applications in the submillimeter radioastronomy," *IEEE Trans. Antennas Propagat.*, vol. 43, no. 12, pp. 1486–1491, 1995.

[4] R. M. Shubair and Y. L. Chow, "Efficient computation of the periodic Green's function in layered dielectric media," *IEEE Trans. Antennas Propagat.*, vol. 41, no. 3, pp. 498–502, 1993.

[5] R. A. Kipp and C. H. Chan, "A numerically efficient technique for the method of moments solution for periodic structures in layered media," *IEEE Trans. Microwave Theory Tech.*, vol. 42, no. 4, pp. 635–643, 1994.

[6] N. Kınayman and M. I. Aksun, "Comparative study of acceleration techniques for integrals and series in electromagnetic problems," *Radio Sci.*, vol. 30, no. 6, pp. 1713–1722, Nov./Dec. 1995.

[7] P. P. Ewald, "Dispersion und Doppelbrechung von Elektronengittern (Kristallen)," Dissertation, München, 1912, also *Ann. Phys. 49*, p. 1, 1916.

[8] P. P. Ewald, "Die Berechnung optischer und elektrostatischer Gitterpotentiale," *Ann. Phys. 64*, pp. 253–287, 1921.

[9] K. E. Jordan, G. R. Richter, and P. Sheng, "An efficient numerical evaluation of the Green's function for the Helmholtz operator on periodic structures," *J. Comp. Phys.*, vol. 63, pp. 222–235, 1986.

[10] A. W. Mathis and A. F. Peterson, "Efficient electromagnetic analysis of a doubly infinite array of rectangular apertures," *IEEE Trans. Microwave Theory Tech.*, vol. 46, no. 1, pp. 46–54, 1998.

[11] H.-Y. D. Yang, R. Diaz, and N. G. Alexopoulos, "Reflection and transmission of waves from multilayer structures with planar implanted periodic material blocks," *J. Opt. Soc. Amer., Ser. B*, vol. 14, no. 10, pp. 2513–2521, Oct. 1997.

[12] S. D. Gedney, J. F. Lee, and R. Mittra, "A combined FEM/MOM approach to analyze the plane wave diffraction by arbitrary gratings," *IEEE Trans. Microwave Theory Tech.*, vol. 40, no. 2, pp. 363–370, 1992.

[13] E. W. Lucas and T. W. Fontana, "A 3-D hybrid finite element/boundary element method for the unified radiation and scattering analysis of general infinite periodic arrays," *IEEE Trans. Antennas Propagat.*, vol. 43, no. 2, pp. 145–153, 1995.

[14] D. T. McGrath and V. P. Pyati, "Phased array antenna analysis with the hybrid finite element method," *IEEE Trans. Antennas Propagat.*, vol. 42, no. 12, pp. 1625–1630, 1994.

[15] D. T. McGrath and V. P. Pyati, "Periodic structure analysis using a hybrid finite element method," *Radio Sci.*, vol. 31, no. 5, pp. 1173–1179, Sept./Oct. 1996.

[16] T. Özdemir and J. L. Volakis, "Triangular prisms for edge-based vector finite element analysis of conformal antennas," *IEEE Trans. Antennas Propagat.*, vol. 45, no. 5, pp. 788–797, 1997.

[17] R. D. Graglia, D. R. Wilton, A. F. Peterson, and I.-L. Gheorma, "Higher order interpolatory vector bases on prism elements," *IEEE Trans. Antennas Propagat.*, vol. 46, pp. 442–450, Mar. 1998.

[18] S. M. Rao, D. R. Wilton, and A. W. Glisson, "Electromagnetic scattering by surfaces of arbitrary shape," *IEEE Trans. Antennas Propagat.*, vol. 30, no. 3, pp. 409–418, 1982.

[19] M. Abramovitz and I. A. Stegun, *Handbook of Mathematical Functions*. New York: Dover, 1965.

[20] D. R. Wilton, S. M. Rao, A. W. Glisson, D. H. Schaubert, O. M. Al-Bundak, and C. M. Butler, "Potential integrals for uniform and linear source distributions on polygonal and polyhedral domains," *IEEE Trans. Antennas Propagat.*, vol. 32, no. 3, pp. 276–281, 1984.

[21] T. F. Eibert and V. Hansen, "On the calculation of potential integrals for linear source distributions on triangular domains," *IEEE Trans. Antennas Propagat.*, vol. 43, no. 12, pp. 1499–1502, 1995.

[22] D. M. Pozar, "The active element pattern," *IEEE Trans. Antennas Propagat.*, vol. 42, no. 8, pp. 1176–1178, 1994.

[23] R. G. Schmier, "The artificial puck frequency selective surface," in *URSI Radio Science Meeting*, Ann Arbor, MI, 1993, p. 266.

Thomas F. Eibert (S'93–M'97) received the Dipl.-Ing. (FH) degree from the Georg-Simon Ohm Fachhochschule, Nürnberg, Germany, in 1989, and the Dipl.-Ing. degree from the Ruhr-Universität Bochum, Bochum, Germany, in 1992, both in electrical engineering. In 1997, he received the Dr.-Ing. degree from the Bergische Universität/GH Wuppertal, Germany.

From 1992 to 1994, he was with the Institut für Hochfrequenztechnik, Ruhr-Universität Bochum, and from 1994 to 1997 he was with the Lehrstuhl für Theoretische Elektrotechnik, Bergische Universität/GH Wuppertal. He is currently working as a Post-Doctoral Fellow under a NATO scholarship from the German Academic Exchange Service (DAAD) at the Radiation Laboratory, Electrical Engineering and Computer Science Department, University of Michigan, Ann Arbor. His research interests include analytical and numerical methods for electromagnetics with emphasis on fast integral algorithms and hybrid formulations combining finite-element methods with integral equation techniques for free space, multilayered media, and periodic structures.

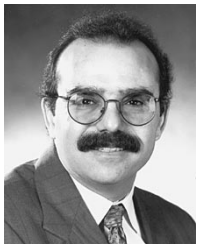

John L. Volakis (S'77–M'82–SM'89–F96) was born in Chios, Greece, on May 13, 1956. He received the B.E. degree (*summa cum laude*) in 1978 from Youngstown State University, Youngstown, OH, the M.Sc. degree in 1979 from the Ohio State University, Columbus, and the Ph.D. degree in 1982, also from the Ohio State University.

He has been with the University of Michigan, Ann Arbor, since 1984 where he is now a Professor in the Department of Electrical Engineering and Computer Science (EECS). He also serves as the Director of the Radiation Laboratory. From 1982 to 1984 he was with Rockwell International, Aircraft Division and during 1978–1982 he was a Graduate Research Associate at the Ohio State University ElectroScience Laboratory. His primary research deals with the development and application of analytical and numerical techniques to large-scale scattering, printed antennas, and bioelectromagnetics. He has published about 150 refereed journal articles, more than 150 conference papers, several book chapters on numerical methods, and coauthored two books: *Approximate Boundary Conditions in Electromagnetics* (IEE, 1995) and *Finite Element Method for Electromagnetics* (IEEE Press, 1998). Along with his students, he develops prototype algorithms for modeling antennas, radar scattering, and imaging of aircraft structures and microwave circuits.

In 1998 , Dr. Volakis received the University of Michigan College of Engineering Research Excellence award. He served as an Associate Editor of the IEEE Transactions on Antennas and Propagation from 1988 to 1992; as an Associate Editor of *Radio Science* from 1994 to 1997; chaired the 1993 IEEE Antennas and Propagation Society Symposium and Radio Science Meeting, and is a current member of the AdCom for the IEEE Antennas and Propagation Society. He now serves as associate editor for the *Journal of Electromagnetic Waves and Applications* and the IEEE Antennas and Propagation Society Magazine. He is a member of Sigma Xi, Tau Beta Pi, Phi Kappa Phi, and Commission B of URSI.

Donald R. Wilton (S63–M'65–SM'80–F'87) was born in Lawton, OK, on October 25, 1942. He received the B.S., M.S., and Ph.D. degrees from the University of Illinois, Urbana-Champaign, in 1964, 1966, and 1970, respectively.

From 1965 to 1968 he was with Hughes Aircraft Co., Fullerton, CA, engaged in the analysis and design of phased array antennas. From 1970 to 1983 he was with the Department of Electrical Engineering, University of Mississippi, and since 1983 he has been Professor of Electrical Engineering at the University of Houston, Houston, TX. During 1978–1979 he was a Visiting Professor at Syracuse University, Syracuse, NY. His research interests are primarily in computational electromagnetics, and he has published, lectured, and consulted extensively in this area.

Dr. Wilton has served the IEEE Antennas and Propagation Society as an Associate Editor of the IEEE TRANSACTIONS ON ANTENNAS AND PROPAGATION, as a Distinguished Lecturer, as a member of AdCom, and currently as Associate Editor of the IEEE Press Series on Electromagnetics. He was also a Guest Co-Editor of a recent special issue of the IEEE TRANSACTIONS ON ANTENNAS AND PROPAGATION devoted to Advanced Numerical Techniques in Electromagnetics. A member of Commission B of URSI, he has served as Secretary, Technical Activities Committee Chair, Vice Chair, and currently as Chair of U.S. Commission B. He has been a U.S. participant in the URSI General Assemblies of 1981, 1984, 1987, 1993, and 1996.

David R. Jackson (S'83–M'84–SM'95–F'99) was born in St. Louis, MO, on March 28, 1957. He received the B.S.E.E. and M.S.E.E. degrees from the University of Missouri, Columbia, in 1979 and 1981, respectively, and the Ph.D. degree in electrical engineering from the University of California, Los Angeles, in 1985.

From 1985 to 1991, he was an Assistant Professor in the Department of Electrical and Computer Engineering at the University of Houston, Houston, TX. Since 1991, he has been an Associate Professor in the same department. His research interests at present include computer-aided design of microstrip antennas and circuits, microstrip antenna analysis and design, periodic structures, leaky-wave antennas, leakage effects in microwave integrated circuits, and bioelectromagnetics.

Dr. Jackson is on the Editorial board of the IEEE TRANSACTIONS ON MICROWAVE THEORY AND TECHNIQUES and the *International Journal of RF and Microwave Computer-Aided Engineering*. He is also an Associate Editor for the IEEE Press Series on Electromagnetic Waves. He is a past Associate Editor for the IEEE TRANSACTIONS ON ANTENNAS AND PROPAGATION. He presently serves as a member of the ADCOM for the IEEE AP-S Society. He also presently serves as the Secretary for URSI U.S. Commission B.